JOURNAL OF GEOPHYSICAL RESEARCH: SPACE PHYSICS, VOL. 118, 3421–3429, doi:10.1002/jgra.50375, 2013

Reduced proton and alpha particle precipitations at Mars during solar wind pressure pulses: Mars Express results

C. Diéval,[1,2] G. Stenberg,[1] H. Nilsson,[1,2] N. J. T. Edberg,[3] and S. Barabash[1]

Received 5 November 2012; revised 21 April 2013; accepted 2 June 2013; published 25 June 2013.

[1] We performed a statistical study of downward moving protons and alpha particles of ~keV energy (assumed to be of solar wind origin) inside the Martian induced magnetosphere from July 2006 to July 2010. Ion and electron data are from the Analyzer of Space Plasma and Energetic Atoms (ASPERA-3) package on board Mars Express. We investigated the solar wind ion entry into the ionosphere, excluding intervals of low-altitude magnetosheath encounters. The study compares periods of quiet solar wind conditions and periods of solar wind pressure pulses, including interplanetary coronal mass ejections and corotating interaction regions. The solar wind ion precipitation appears localized and/or intermittent, consistent with previous measurements. Precipitation events are less frequent, and the precipitating fluxes do not increase during pressure pulse encounters. During pressure pulses, the occurrence frequency of observed proton precipitation events is reduced by a factor of ~3, and for He^{2+} events the occurrence frequency is reduced by a factor of ~2. One explanation is that during pressure pulse periods, the mass loading of the solar wind plasma increases due to a deeper penetration of the interplanetary magnetic flux tubes into the ionosphere. The associated decrease of the solar wind speed thus increases the pileup of the interplanetary magnetic field on the dayside of the planet. The magnetic barrier becomes thicker in terms of solar wind ion gyroradii, causing the observed reduction of H^+/He^{2+} precipitations.

Citation: Diéval, C., G. Stenberg, H. Nilsson, N. J. T. Edberg, and S. Barabash (2013), Reduced proton and alpha particle precipitations at Mars during solar wind pressure pulses: Mars Express results, *J. Geophys. Res. Space Physics*, *118*, 3421–3429, doi:10.1002/jgra.50375.

1. Introduction

[2] The Martian ionosphere presents a partially conductive obstacle to the solar wind. When flowing around Mars, the solar wind, which carries the frozen-in interplanetary magnetic field (IMF), induces currents in the ionosphere. At the same time, the IMF diffuses into the ionosphere. There is a superposition of the magnetic fields from the induced currents, and the IMF partially diffused into the ionosphere. This superposition creates a region of an increased magnetic field above the ionosphere, the so-called magnetic barrier.

[3] The inner edge of the magnetic barrier corresponds to the photoelectron boundary (PEB), below which the ionosphere starts and where the ionospheric electron density steeply increases [*Frahm et al*., 2006; *Dubinin et al*., 2008]. The outer edge of the magnetic barrier is referred to as the induced magnetospheric boundary (IMB) [*Dubinin et al*., 2006]. There is a pressure balance at the IMB between the upstream dynamic pressure and the magnetic pressure of the pileup region. The IMB also separates the solar wind ions (mainly H^+, He^{2+}) from the planetary ionospheric ions (mainly O^+, O_2^+, CO_2^+) [e.g., *Breus et al*., 1991].

[4] However, in some circumstances, solar wind ions are able to pass from the magnetosheath to the ionosphere. In the hot magnetosheath plasma, there are solar wind ions with a gyroradius comparable to the size of the subsolar magnetic barrier. For example, the gyroradius for a typical 1 keV solar wind proton H^+ and for a typical 4 keV solar wind alpha particle He^{2+} are 152 km and 306 km, respectively, for a background magnetic field strength of 30 nT (a typical strength of the dayside piled up magnetic field). These gyroradii are close to the nominal size of the subsolar magnetic barrier, estimated to be 300 km, using the mean altitude of the PEB at 400 km from *Mitchell et al*. [2001] and the mean altitude of the subsolar IMB at 700 km from *Dubinin et al*. [2006]. Modeling studies predict that solar wind ions with relatively high energies (large gyroradii) can cross the IMB without being deflected away and that they finally travel down, i.e., precipitate to low altitudes [*Brecht*, 1997; *Kallio and Janhunen*, 2001]. The precipitating protons and alpha particles then deposit their energy into the Martian upper atmosphere, causing charge exchange reactions, momentum transfer, ionization, and heating of the planetary neutral atoms [*Kallio and Janhunen*, 2001; *Shematovich et al*.,

[1]Swedish Institute of Space Physics, Kiruna, Sweden.
[2]Division of Space Technology, Department of Computer Science, Electrical and Space Engineering, Luleå University of Technology, Kiruna, Sweden.
[3]Swedish Institute of Space Physics, Uppsala, Sweden.

Corresponding author: C. Diéval, Swedish Institute of Space Physics, Box 812, SE-98128 Kiruna, Sweden. (catherine@irf.se)

2169-9380/13/10.1002/jgra.50375

2011, 2013]. Downgoing protons and alpha particles with solar wind energies are regularly observed in the Martian ionosphere but found to be localized and/or intermittent [*Lundin et al*., 2004; *Stenberg et al*., 2011; *Diéval et al*., 2012a, 2013].

[5] There are two main types of solar disturbance of the interplanetary medium associated with high dynamic pressures: the corotating interaction regions (CIR) and the interplanetary coronal mass ejections (ICME).

[6] CIRs are recurrent structures of the interplanetary medium [see, e.g., *Hundhausen*, 1972]. The rotating and tilted Sun emits fast plasma at the poles and slow plasma near the equator. The fast solar wind stream overtakes the slow solar wind stream, forming the CIR. The CIR is a spiral structure which rotates with the Sun.

[7] Coronal mass ejections are sporadic ejections of huge amounts of plasma and twisted magnetic field lines from the Sun. ICMEs correspond to the propagation of this material in the interplanetary medium [see, e.g., *Jian et al*., 2006].

[8] When a solar wind pressure pulse impacts Mars, the resulting intense solar wind fluxes move closer to the planet, tailward fluxes of accelerated planetary ions are enhanced, and atmospheric escape increases [e.g., *Dubinin et al*., 2009; *Edberg et al*., 2010; *Nilsson et al*., 2011]. Modeling studies also indicate increased atmospheric escape during high dynamic pressure conditions compared to quiet conditions [e.g., *Harnett and Winglee*, 2006; *Kaneda et al*., 2009].

[9] *Hara et al*. [2011] reported observations of enhanced fluxes of O^+ ions picked up by the solar wind, precipitating at the Martian terminator, during solar wind pressure pulses. Under normal solar conditions, the picked up O^+ ions have gyroradii larger than the planet (Martian radius = 3397 km) and are quickly swept away by the solar wind. However, during conditions of high upstream dynamic pressure and/or high IMF strength, the magnetic pressure increases in the Martian pileup region, and the gyroradii of the picked up ions decrease [*Hara et al*., 2011], so that these ions are more likely to impact the planet along their trajectory.

[10] In this paper, we investigate how the precipitating H^+ and He^{2+} ions react to pressure pulses. Section 2 presents the instrumentation and the methodology. Section 3 describes the results. Section 4 discusses the results in relation to previous work. Section 5 concludes the paper.

2. Instrumentation and Data Selection

[11] We use in situ ion and electron measurements from the Analyzer of Space Plasma and Energetic Atoms (ASPERA-3) package [*Barabash et al*., 2006] onboard the Mars Express (MEX) spacecraft. We use the Electron Spectrometer (ELS) and the Ion Mass Analyzer (IMA). ELS measures 2-D distributions of the electron flux in the energy range 5 eV to 15 keV with a field of view of 4° × 360° divided into 16 azimuth sectors and a time resolution of 4 s. IMA measures distributions of the fluxes of different ion species, including H^+, He^{2+}, and O^+, with m/q resolution in the energy range 200 eV/q to 36 keV/q. In practice, the lower energy limit to detect protons is ~1.2 keV for the intermediate postacceleration level. The postacceleration voltage serves to vary the mass resolution of the instrument (see details in *Barabash et al*. [2006]). IMA gives a 2-D measurement of the ion fluxes (16 azimuth sectors), for all energies, at a time resolution of 12 s. A full distribution with a field of view of 90° × 360° is obtained in 192 s (one IMA scan), using electrostatic sweeping to get ±45° coverage out of the plane of the aperture (sweep over elevation angles). We use data from July 2006 to July 2010 (during the solar minimum) except May 2007 and November 2009 when new IMA energy tables were uploaded. We consider altitudes from ~260 km (pericenter) up to 2000 km, in the region $X_{MSO} > 0$ (dayside). In the Mars Solar Orbital (MSO) Cartesian coordinate system, the X_{MSO} axis points from the center of Mars toward the Sun, the Y_{MSO} axis points opposite to the Martian orbital velocity vector, and the Z_{MSO} axis completes the right-handed system.

[12] We are only interested in precipitation events observed inside the ionosphere, below the PEB. We have manually identified and selected IMA scans presenting proton and alpha particle fluxes (with ~keV energy) in the presence of ionospheric photoelectrons and in the absence of magnetosheath electrons. The method is the same as used by *Diéval et al*. [2013]. A proton (alpha particle) precipitation event corresponds to an IMA scan during which a downward integrated proton (alpha particle) flux exists, i.e., a precipitating flux. We exclude from the consideration time periods when the data were regarded invalid (instrumental effects, etc.). We remove precipitation events showing severe contamination by ultraviolet radiation or by other ion species. To separate solar wind alpha particles from low-energy planetary H_2^+ (both have m/q = 2, where m is the ion mass and q the elementary charge), we consider the mass line m/q = 2 for energies above 200 eV only.

[13] The measurements take place at altitudes >260 km, well above the altitude of the exobase at solar minimum, ~180 km. Thus, we cannot be sure that the measured precipitating ions will reach the exobase further down and finally be lost in the atmosphere. For example, ions moving downward at a given time may, through the Lorentz force, end up moving upward at a later time and not reach the exobase at all. Conversely, ions moving upward may end up moving downward and finally reach the exobase. We then need to know the electromagnetic environment to which the ions are subject: this is a modeling task [see, e.g., *Fang et al*., 2010], beyond the scope of the paper. We just consider downward ion fluxes in this study and assume that these ions reach the exobase.

[14] We treat proton events and alpha particle events independently, and we do not attempt to examine the differences in solar wind ion composition during different sets of external conditions. We note that the data coverage (total number of IMA scans during the period of study, including the precipitation events) is slightly different for the proton study and the alpha particle study. This is because, for each separate study, we removed from the data coverage the scans which were identified as potential precipitation events but were finally discarded due to severe contamination by ultraviolet radiation or by other ion species.

[15] We use an extended version of the list of solar wind pressure pulse encounters with Mars (ICMEs and CIRs) determined by *Edberg et al*. [2010]. *Edberg et al*. [2010] describe in detail the automatic selection of solar wind pressure pulse intervals from the magnetic field and ion data measured by the Advanced Composition Explorer (ACE) spacecraft, which monitors the solar wind upstream of the Earth. The arrival time at Mars of such solar wind pressure

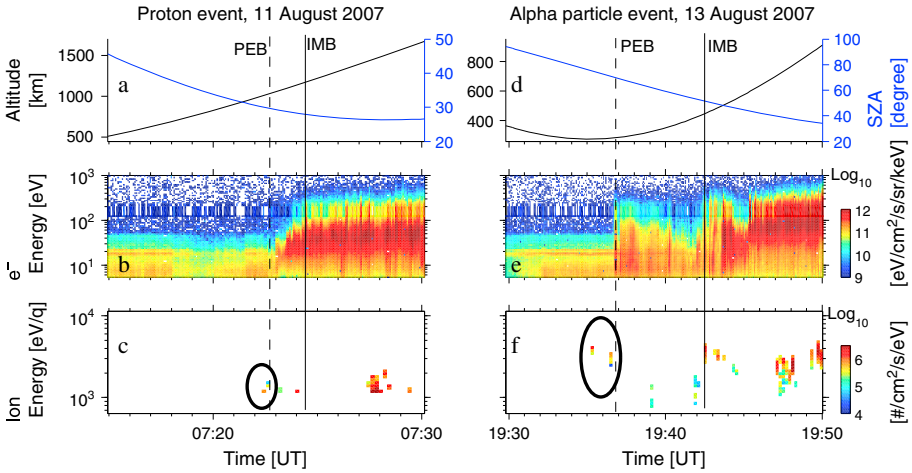

Figure 1. (left) A proton precipitation event on 11 August 2007. The vertical solid line marks the IMB crossing, and the vertical dashed line marks the PEB crossing. (a) Altitude of MEX (black curve, left axis) and SZA of MEX (blue curve, right axis). (b) Energy-time spectrogram of electrons measured by ELS (averaged over all sectors). (c) Energy-time spectrogram of protons measured by IMA (downward flux summed over sectors). (right) An alpha particle precipitation event on 13 August 2007. The format is the same as for Figure 1 (left), except that Figure 1f shows alpha particles.

pulse is calculated following the method of *Vennerstrom et al.* [2003] [see *Edberg et al.*, 2010]. This calculated time is then compared with the electron observations from MEX to get a more accurate arrival time as well as an end time of the pressure pulse encounter, which we use in this work. During the observation period, 121 automatically selected ICMEs/CIRs had counterparts in the MEX data at Mars (no large gap in MEX data). To this list, we add 72 intervals manually selected in the MEX data, suggesting an ICME/CIR passage. For these 72 intervals, we manually check for counterparts in the ACE data: either no counterpart can be found (cases of an ICME hitting only MEX but not ACE) or a counterpart is identified by eye in the ACE data but does not meet the automatic selection criterion. The full list contains 193 intervals of solar wind pressure pulse encounters at Mars. Finally, we check the intervals for valid dayside IMA data below the local PEB. The final numbers of pressure pulse intervals are 150 for the proton study and 149 for the alpha particle study, respectively.

[16] Finally, we do not consider the solar radiation environment in this study, i.e., ion fluxes with energies from tens of keV to GeV. These energies are beyond the upper energy limit of the IMA instrument, 36 keV/q. Note that the detection efficiency of IMA is poor at the high end of its energy range.

3. Observations

[17] Examples of precipitating H^+ and He^{2+} are shown in Figure 1. The left column shows a proton event (Figures 1a, 1b, and 1c) on 11 August 2007 from 0715 to 0730 UT, during orbit # 4627. The dayside ionosphere electron spectra are characterized by narrow photoelectron peaks (horizontal lines between 20 and 30 eV, *Frahm et al.* [2006]) between 0715 and ~0723 UT in Figure 1b. The proton precipitation event is detected in the ionosphere at 0722 UT (altitude ~1000 km, solar zenith angle (SZA) = 29°, energy range 1.1–1.7 keV). The PEB is crossed outbound at ~0723 UT. The IMB is crossed outbound at 0724 UT (SZA = 28°, altitude ~1100 km). Afterward, the magnetosheath plasma is recognized by high fluxes of electrons at suprathermal energies (40–300 eV). This case shows clear crossings of the plasma boundaries, suggesting quiet solar wind conditions.

[18] The right column of Figure 1 shows an alpha particle event (Figures 1d, 1e, and 1f), on 13 August 2007 from 1930 to 1950 UT, during orbit # 4636. The dayside ionosphere is visible from 1930 to ~1937 UT (Figure 1e). The precipitating He^{2+} event is detected at 1935–1936 UT in the ionosphere (altitude ~580–620 km, SZA ~43–44°, energy = 3 keV/q). Between ~1937 and ~1943 UT, there are multiple crossings of the ionosphere/magnetosheath interface, where we see both ionospheric photoelectrons and reduced fluxes of shocked electrons: this is the magnetic pileup region. This result suggests unsteady solar wind conditions and makes the identification of plasma boundary crossings difficult. We choose to place the outbound PEB crossing at ~1937 UT and the outbound IMB crossing at ~1943 UT (SZA = 52°, altitude = 440 km). The IMB crossing occurs at low altitude on 13 August, compared to the crossing on 11 August: the magnetosphere was more compressed than usual. The magnetosheath is present from ~1943 UT. There is a dip in the suprathermal electron flux between 1944 and 1945 UT, indicating that the plasma boundaries moved to higher altitudes during this interval, likely because of a short-duration decrease of the upstream dynamic pressure. The disturbed solar wind conditions shown by the MEX data on 13 August 2007 are the results of a CIR encounter with Mars. The same CIR front reached the ACE spacecraft earlier on 6 August 2007.

[19] Figure 2 gives an overview of the passage of this CIR at Earth and then at Mars. Figures 2a, 2b, 2c, and 2d are time series of ACE data showing the IMF strength, the density, the bulk velocity, and the dynamic pressure of the solar wind

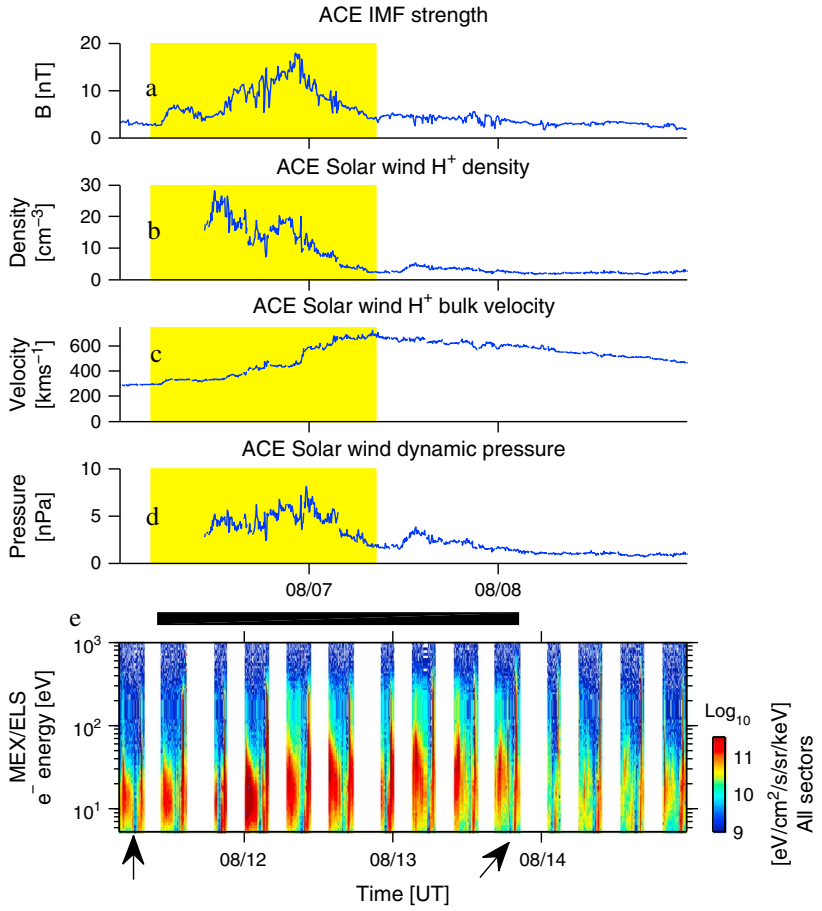

Figure 2. Time series of ACE data. (a) IMF strength. (b) Solar wind proton density. The density until 6 August 2007 at 1100 UT is poorly determined and is not shown. (c) Solar wind proton bulk velocity. (d) Solar wind proton dynamic pressure. The period of the CIR encounter with ACE is indicated by the yellow shading, from 6 August 2007 (0400 UT) to 7 August 2007 (0830 UT). (e) Electron energy-time spectrogram (averaged over all sectors) observed by MEX. The white vertical bands are data gaps corresponding to no data taking when the spacecraft is sufficiently far away from the Martian bow shock. The estimated period of the CIR encounter with Mars is indicated by a horizontal black bar, from 11 August 2007 (~0930 UT) to 13 August 2007 (~2300 UT). The times of the two precipitation events previously discussed are indicated by arrows.

protons, respectively, from 6 August 2007 (0000 UT) to 9 August 2007 (0000 UT). The magnetic field is given by the MAGnetometer MAG [*Smith et al.*, 1998], and the solar wind parameters are given by the Solar Wind Electrons, Protons, and Alpha Particle Monitor [*McComas et al.*, 1998]. At the beginning of the interval, the solar wind conditions are quiet: IMF strength = 4 nT, and solar wind bulk velocity = 290 km s^{-1}. On 6 August 2007 at 0400 UT, the spacecraft meets the CIR front. During the passage of the CIR, there are increases of the solar wind density (up to 26 cm^{-3}), of the IMF strength (up to 18 nT), and of the dynamic pressure (up to 8 nPa), followed by a decline of these parameters down to their nominal values at the end of the CIR encounter, on 7 August 2007 at 0830 UT. CIRs are indeed characterized by high values of the magnetic field strength, plasma density, and dynamic pressure. Inside the CIR, the solar wind bulk speed increases more gradually to finally reach a maximum value of ~690 km s^{-1} (Figure 2c). After the passage of the CIR, the bulk velocity slowly decreases during several days.

[20] Figure 2e is an electron energy-time spectrogram measured by MEX, from 11 August 2007 (0350 UT) to 14 August 2007 (2332 UT). The panel shows low-altitude data intervals measured during 14 consecutive orbits (the orbit is elliptical). The estimated period of the impact of the pressure pulse is indicated by a horizontal black bar from 11 August 2007 (~0930 UT) to 13 August 2007 (~2300 UT) by visual identification. Indeed, the electron distribution is hotter and the flux more intense during this period compared to the periods before and after the CIR passage. The times of the two precipitation events previously discussed are marked by arrows. The proton event on 11 August 2007 occurred during the quiet upstream conditions which preceded the impact of the CIR front at Mars. The He^{2+} event occurred on 13 August 2007 when the upstream conditions were still disturbed at the end of the passage of the CIR.

[21] Next, we compare the H^+ and He^{2+} precipitation events during the two regimes of upstream conditions. Figure 3 shows the IMA data coverage (that is the number of IMA scans) below the local dayside PEB, in the X_{MSO}-R_{MSO} plane,

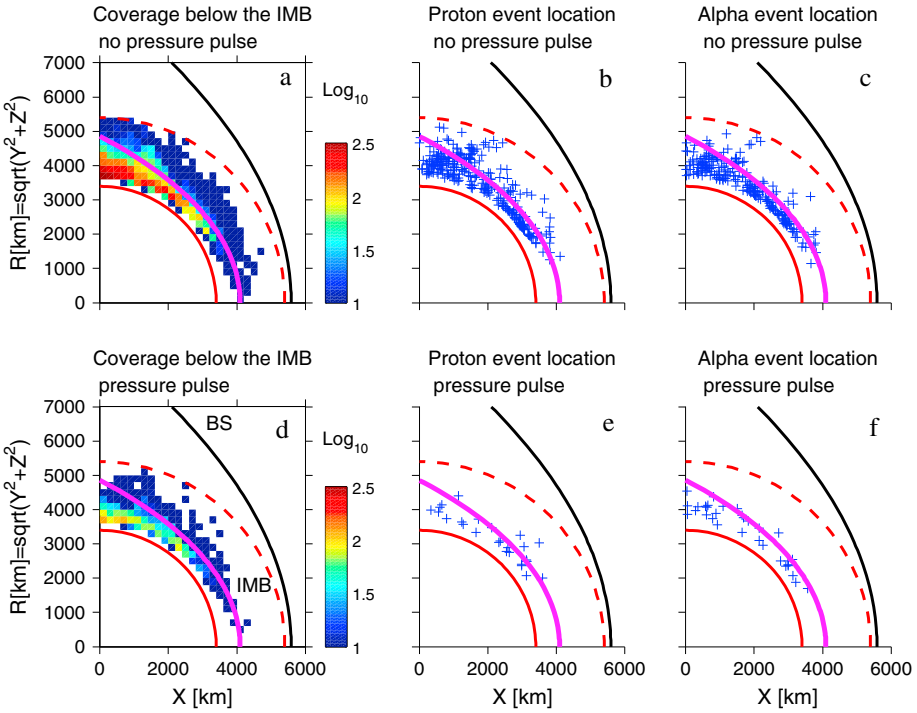

Figure 3. The X_{MSO}-R_{MSO} plane. The horizontal axis is the distance along the Mars Sun line. The vertical axis is the distance $R_{MSO} = \sqrt{Y_{MSO}{}^2 + Z_{MSO}{}^2}$ from the Mars Sun line. The spatial bin size is 200 km × 200 km. The red solid curve, the black solid curve, and the magenta solid curve indicate Mars, the bow shock model of *Vignes et al.* [2000], and the IMB model of *Dubinin et al.* [2006], respectively. The red dashed curve shows the altitude limit of 2000 km below which data were considered. (top) Periods of quiet solar wind. (bottom) Periods during solar wind pressure pulses. (a and d) Data coverage below the PEB, excluding invalid scans. The color bar indicates the number of IMA scans obtained in each spatial bin. (b, e, c, and f) Location of the precipitation events indicated by plus symbols.

for the proton study. Figure 3a shows the data during quiet conditions, and Figure 3d shows the data during pressure pulses. The data coverage for the alpha particle study is similar and is not shown. The ICMEs/CIRs represent 22.6% of the data coverage, and the quiet upstream conditions represent the rest. *Edberg et al.* [2010] estimated that pressure pulses impacted Mars during ~15% of the time. However, we also include pressure pulse intervals at Mars which were not identified by the automatic selection used by *Edberg et al.* [2010], thus increasing our proportion of pressure pulse periods. Table 1 summarizes the data coverage during both sets of solar wind conditions, for the proton and alpha particle studies.

[22] As seen from Figure 3 (Figures 3a and 3d), the coverage below the PEB is best at low altitudes around the terminator. The blue pixels above the IMB model of *Dubinin et al.* [2006] (the magenta curve in the figure) indicate that the spacecraft sometimes samples the ionosphere at altitudes above the model, because the altitude of the PEB changes with varying solar wind conditions. Of the data coverage, 0.3% occurs at altitudes >1900 km.

[23] The spatial location of the precipitation events in the X_{MSO}-R_{MSO} plane during quiet solar wind conditions is shown in the top row (Figure 3b, protons and Figure 3c, alpha particles) and during pressure pulses in the bottom row (Figure 3e, protons and Figure 3f, alpha particles). Most of the proton and alpha particle events are located below the position of the IMB model, while a few events can also be found above the model, since we consider all observations below the locally observed PEB, and thus IMB. The events are found at both low altitudes and high altitudes during quiet external conditions. The altitude range of the events is restricted to low altitudes during pressure pulse encounters because the induced magnetosphere is compressed. Fewer events are detected during periods of disturbed external conditions.

Table 1. IMA Data Coverage Below the Local PEB and Excluding Invalid Scans[a]

	During Quiet Conditions	During Pressure Pulses	Total
	Proton Study		
Number of scans	8452	2474	10,926
% of scans	77.4	22.6	100.0
	Alpha Particle Study		
Number of scans	8348	2466	10,814
% of scans	77.2	22.8	100.0

[a]The data coverage during quiet solar wind conditions and during ICMEs/CIRs passages is given separately for the H^+ study and the He^{2+} study.

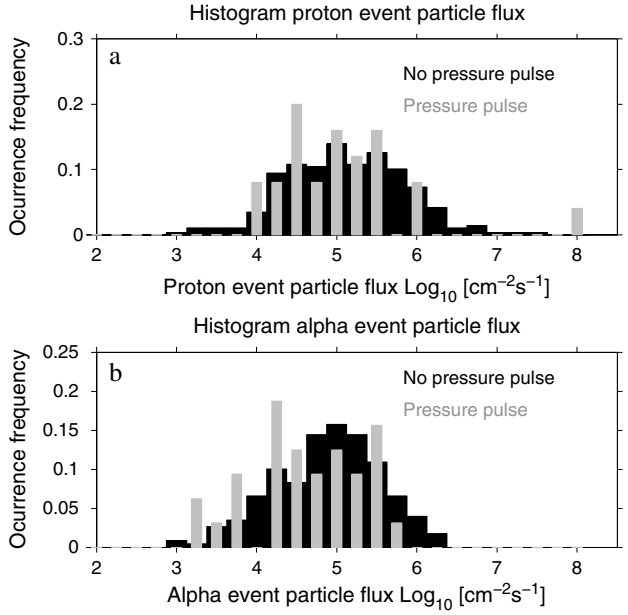

Figure 4. Histograms of the particle flux (a) of the proton precipitation events and (b) of the alpha particle precipitation events. The black-shaded histogram and the gray-shaded histogram correspond to periods during quiet conditions and periods during solar wind pressure pulses, respectively. Each distribution is normalized by the total number of samples of the population. The gray-shaded bin on the far right in Figure 4a contains one outlier event with a flux of $8.1 \cdot 10^7\,\mathrm{cm}^{-2}\,\mathrm{s}^{-1}$.

[24] We have examined the distribution of downward particle fluxes for the proton events and for the alpha particle events, comparing periods of quiet external conditions with periods of disturbed external conditions. Figure 4 shows histograms of the particle flux for the proton events (Figure 4a) and for the alpha particle events (Figure 4b). The black-shaded distribution corresponds to the quiet upstream conditions, and the gray-shaded distribution corresponds to the CIR/ICME passages.

[25] Figure 4a shows that the shape of the distribution of fluxes of the proton precipitation events is similar during quiet external conditions and during pressure pulses, both ranging from 10^4 to $10^6\,\mathrm{cm}^{-2}\,\mathrm{s}^{-1}$, although the statistics are poorer in the case of the pressure pulse periods due to the small number of events. During quiet and disturbed upstream conditions, the median values of the proton event flux are $1.2 \cdot 10^5\,\mathrm{cm}^{-2}\,\mathrm{s}^{-1}$ and $8.6 \cdot 10^4\,\mathrm{cm}^{-2}\,\mathrm{s}^{-1}$, respectively. Figure 4b in Figure 4 shows that the distributions of the fluxes of the alpha particle events have a similar shape during quiet external conditions and during pressure pulses, and both range from $10^3\,\mathrm{cm}^{-2}\,\mathrm{s}^{-1}$ to $10^6\,\mathrm{cm}^{-2}\,\mathrm{s}^{-1}$. The statistics are again poorer in the case of the pressure pulse periods. During quiet and disturbed upstream conditions, the median values of the alpha particle event flux are $8.8 \cdot 10^4\,\mathrm{cm}^{-2}\,\mathrm{s}^{-1}$ and $4.3 \cdot 10^4\,\mathrm{cm}^{-2}\,\mathrm{s}^{-1}$, respectively.

Table 2. Distribution of Solar Wind Pressure Pulses According to the Presence or Absence of Precipitating H^+ Events and He^{2+} Events

	With H^+ Events	No H^+ Events	Total
Number of pressure pulses	17	133	150
% of pressure pulses	11.3	86.7	100.0
	With He^{2+} Events	No He^{2+} Events	Total
Number of pressure pulses	21	128	149
% of pressure pulses	14.0	86.0	100.0

[26] We have used a Student's *t* test (assuming unequal and unknown variances) to compare the two distributions (event fluxes during quiet periods and disturbed periods) for both the proton study and the alpha particle study. The test shows no significant difference between the two distributions (the probability p value is 0.7 for the proton study and 0.06 for the alpha particle study). We conclude that the H^+ and He^{2+} event fluxes do not increase during solar wind disturbances.

[27] We also calculate the occurrence frequency of detecting H^+ and He^{2+} events during quiet solar wind conditions and during ICME/CIR passages. Tables 2, 3a, 3b, 4 summarize the occurrence frequency and typical fluxes of the proton events and alpha particle events during both sets of upstream conditions.

[28] For the protons, the occurrence frequencies are 1.01% during ICMEs/CIRs encounters and 3.39% during quiet conditions (Table 3a). The occurrence frequency is a factor of ~3 lower during disturbed solar wind conditions. The majority of pressure pulses contain no proton event (Table 2), while the pressure pulse intervals represent on average ~23% of the data coverage (Table 1).

[29] For the alpha particles, the occurrence frequencies are 1.30% during ICMEs/CIRs encounters and 2.75% during quiet conditions (Table 3b). The occurrence frequency is a

Table 3a. Distribution of Precipitating Proton Events During Pressure Pulses and During Quiet Solar Wind Conditions

	Number of Events	% of Events	Occurrence Frequency Relative to the Period[a] (%)	Average Particle Flux [b] ($\mathrm{cm}^{-2}\,\mathrm{s}^{-1}$)	25th Percentile Particle Flux ($\mathrm{cm}^{-2}\,\mathrm{s}^{-1}$)	Median Particle Flux ($\mathrm{cm}^{-2}\,\mathrm{s}^{-1}$)	75th Percentile Particle Flux ($\mathrm{cm}^{-2}\,\mathrm{s}^{-1}$)
ICMEs/ CIRs	25	8.0	1.01	$1.1 \cdot 10^5$	$2.6 \cdot 10^4$	$8.6 \cdot 10^4$	$2.7 \cdot 10^5$
Quiet conditions	287	92.0	3.39	$1.3 \cdot 10^5$	$4.0 \cdot 10^4$	$1.2 \cdot 10^5$	$4.2 \cdot 10^5$
Total events	312	100.0	2.85	$1.3 \cdot 10^5$	$3.8 \cdot 10^4$	$1.2 \cdot 10^5$	$4.0 \cdot 10^5$

[a]The occurrence frequency of detecting the proton events is calculated for each period using the number of proton events divided by the number of IMA scans of the data coverage.

[b]The mean values of the downward particle flux of the proton events are calculated as 10^(mean($\log_{10}$(fluxes))).

Table 3b. Distribution of Precipitating Alpha Particle Events During Pressure Pulses and During Quiet Solar Wind Conditions[a]

	Number of Events	% of Events	Occurrence Frequency Relative to the Period (%)	Mean Particle Flux ($cm^{-2} s^{-1}$)	25th Percentile Particle Flux ($cm^{-2} s^{-1}$)	Median Particle Flux ($cm^{-2} s^{-1}$)	75th Percentile Particle Flux ($cm^{-2} s^{-1}$)
ICMEs/ CIRs	32	12.3	1.30	$4.1 \cdot 10^4$	$1.5 \cdot 10^4$	$4.3 \cdot 10^4$	$1.6 \cdot 10^5$
Quiet conditions	229	87.7	2.74	$7.4 \cdot 10^4$	$2.5 \cdot 10^4$	$8.7 \cdot 10^4$	$2.1 \cdot 10^5$
Total events	261	100.0	2.41	$6.9 \cdot 10^4$	$2.3 \cdot 10^4$	$8.0 \cdot 10^4$	$2.0 \cdot 10^5$

[a]Same format as in Table 3a.

factor of ~2 lower during disturbed solar wind conditions. Here again, the majority of the pressure pulses contain no alpha particle event (Table 2).

[30] The data set during disturbed conditions is roughly 4 times smaller than the data set during quiet conditions. We thus need to check whether the difference in occurrence frequency is significant. For this purpose, we compare the results during pressure pulses with intervals of similar number of IMA scans drawn from the period of quiet conditions. We take four intervals of 2000 scans each. The occurrence frequency calculated from chronological intervals is biased by the orbit geometry, which evolves over time. Instead, we take random intervals, and we calculate the median occurrence frequency of detecting the precipitation events in these intervals. When comparing the results, we assume that the CIR/ICMEs regularly impact Mars during short periods of arbitrary orbital geometry and that this data set can be considered as a random group.

[31] The median occurrence frequency for the proton events during quiet conditions is 3.45%: this is a factor of ~3 larger than the occurrence frequency of 1.01% during pressure pulses. The median occurrence frequency for the alpha particle events during quiet conditions is 2.70%: this is a factor of ~2 larger than the occurrence frequency of 1.30% during pressure pulses. Therefore, there is a significant difference in the occurrence frequency of measuring the H^+ and He^{2+} events during quiet solar wind conditions and during ICME/CIR passages. The results are summarized in Table 4.

4. Discussion

[32] We have conducted a study of keV-energy proton and alpha particle precipitations in the Martian upper atmosphere, during periods of quiet solar wind and disturbed solar wind, using 4 years of Mars Express data near the solar minimum. Such solar wind energies suggest a solar wind origin [*Lundin et al*., 2004; *Diéval et al*., 2012a, 2013; *Stenberg et al*., 2011]. For the protons in particular, solar wind protons and planetary protons picked up from the hydrogen corona can both contribute significantly to the proton precipitation, with a major part (~60%) coming from the solar wind, according to the modeling work by *Diéval et al*. [2012a, 2012b]. We cannot separate the origins of the precipitating protons with our measurements, and we just assume that both origins contribute, especially the solar wind.

Table 4. Median Occurrence Frequency of Measuring Precipitating H^+ and He^{2+} Events During Periods of Quiet Solar Wind, Calculated From Four Random Groups of Scans Drawn From the Data Set, as Explained in the Text

	No Pressure Pulses	Pressure Pulses [a]
Occurrence frequency of H^+ events (%)	3.45	1.01
Occurrence frequency of He^{2+} events (%)	2.70	1.30

[a]The occurrence frequency of measuring the events during pressure pulses is also repeated from Tables 3a and 3b.

[33] We do not observe the proton events and alpha events during every ionospheric pass by MEX. If we do observe them during a given pass, it is only during a part of the pass, just below the plasma boundaries and rarely near the pericenter. For example, *Stenberg et al*. [2011] report detecting precipitating alpha particles during 22% of the dayside ionospheric passes they investigated. And *Diéval et al*. [2013] report precipitating protons detected only 3% of the observation time in the dayside ionosphere. Precipitation events appear localized and/or isolated. There are two possible scenarios. Either the ion precipitation may be global but appears local to an observer if it is intermittent (observed part of the time), or the ion precipitation may be permanent but appears local to an observer if it is localized in space. The precipitation may even be both intermittent and spatially localized, and we cannot separate time variations from space variations with a single spacecraft.

[34] We do not know what triggers the intermittent ion precipitation. A possible mechanism is transient increases in magnetosheath ion temperature, causing transient increases in ion gyroradius [*Diéval et al*., 2012a, 2013]. This could allow a part of the magnetosheath ion population to gyrate through the magnetic barrier due to large gyroradii and then reach the ionosphere.

[35] The localized and/or intermittent solar wind ion precipitation disagrees with the global permanent precipitation state indicated by models [e.g., *Kallio and Janhunen*, 2001; *Chanteur et al*., 2009]. We note that *Hara et al*. [2011] also observed intermittent cases of heavy ion precipitation while models predict that it occurs at any time [e.g., *Chaufray et al*., 2007]. In addition, models [e.g., *Kallio and Janhunen*, 2001] tend to overestimate the fluxes of precipitating protons by 1–2 orders of magnitude compared to the measured values.

[36] Several instrumental factors can contribute to reduce or even miss the fluxes of observed protons and alpha particles. During 40 min around pericenter, MEX is in the nadir pointing mode, and then IMA's central plane is oriented such

that it can measure upgoing and downgoing ions. However, the field of view is not 4π, and this can contribute to underestimating ion fluxes. On the other hand, *Diéval et al*. [2012a] report rather broad angular distributions for protons observed in the Martian ionosphere (several IMA angular sectors), so it is unlikely to miss events of proton precipitation due to this limitation. In addition, for proton measurements, the instrumental energy threshold prevents the detection of protons with energies <700 eV (most favorable case, when IMA is run in the highest postacceleration voltage), and this may lead to underestimate the fluxes or even to miss proton events in some cases. However, the observed proton events have mean energies of typically 1–2 keV [*Diéval et al*., 2013], and in this case, the maximum in flux is at energies above the energy threshold of 700 eV. In addition, the relatively high background level of IMA may hide weak ion signals and prevent their detection. A number of potential precipitation events were also discarded in this study due to severe contamination by ultraviolet radiation or by other ion species. Finally, a single spacecraft performing in situ measurements can be only at a certain place at a certain time and may miss precipitation events if they are localized in space.

[37] On the other hand, the hybrid models have also their limitations. The large grid cells prevent an accurate description of the near-Mars environment, and localized ion precipitation zones may not be resolved. Furthermore, the time-stationary inputs to the simulations do not allow reproducing time-dependent phenomena such as the intermittent ion precipitation. Finally, models lack an accurate description of the atmosphere/ionosphere; for example, they may use a spherical conductive ionosphere without implementing chemical reactions. In the case of the model of *Brecht* [1997], there is even no atmosphere/ionosphere included. The models produce more ion precipitation than they should. We think that solving the discrepancies between models and measurements will come in great part from the improvement of current models.

[38] The occurrence frequency of detecting the precipitating solar wind ions is significantly lower during pressure pulses than during quiet conditions. Although the magnetosheath flux is observed to be larger and to reach lower altitudes during the passage of pressure pulses [e.g., *Dubinin et al*., 2009], we find that the precipitating flux itself does not increase. This result means that a smaller fraction of the upstream solar wind flux can precipitate under these conditions, contrary to modelers' expectations [*Brecht*, 1997; *Harnett and Winglee*, 2006], and suggests that the magnetic barrier is a more effective obstacle to the H^+ and He^{2+} precipitation during pressure pulses. We recall that we take the H^+ and He^{2+} events within the ionosphere, clearly below the IMB. The precipitation events we are looking for are thus not related to the motion of plasma boundaries but to the crossing of boundaries by some precipitating ions.

[39] The effectiveness of the magnetic barrier as an obstacle to the H^+ and He^{2+} precipitation is determined by the thickness of the magnetic barrier in terms of H^+ gyroradii and He^{2+} gyroradii. The thickness in terms of ion gyroradii depends on the total magnetic flux in the magnetic barrier. If the total magnetic flux is constant in the magnetic barrier, then a thinner magnetic barrier leads to a higher magnetic field strength and to smaller ion gyroradii, but the thickness of the obstacle in terms of ion gyroradii remains approximately the same.

[40] The total magnetic flux should increase with respect to quiet upstream conditions in the magnetic barrier during a pressure pulse to explain the lesser solar wind ion precipitation. We suggest that this is possible when the magnetosheath flow is decelerated by a stronger mass loading under these conditions. The increased magnetic field in the magnetic barrier region penetrates deeper into the ionosphere (we assume no change in the ionosphere conductivity during the pressure pulse events). Therefore, the magnetic field tubes are dragged through the ionosphere layers with higher ion density and, thus, get more loaded by the planetary ions, mostly O^+. This results in the increase of the ionospheric erosion and the total ion escape, indeed, reported by modelers [e.g., *Kaneda et al*., 2009] and observers [e.g., *Edberg et al*., 2010, 2011]. The additional mass of planetary ions into the solar wind causes a deceleration of the solar wind at low altitudes due to the conservation of momentum [e.g., *Dubinin et al*., 2000]. The solar wind magnetic field, frozen-in into the plasma flow, takes a longer time to sweep past the planet. The IMF piles up even more on the dayside before it is convected to the nightside, leading to a larger total magnetic flux in the magnetic barrier. Furthermore, the IMF strength in the upstream solar wind is typically larger than usual (several tens of nT), and this also can contribute to increase the total magnetic flux in the magnetic barrier. Measurements by the Mars Global Surveyor orbiter indeed showed an enhanced magnetic field strength in the magnetic barrier during solar wind disturbances [e.g., *Crider et al*., 2005]. Also, models indicate that the magnetic barrier is more developed during conditions of high IMF strength and high dynamic pressure, [e.g., *McKenna-Lawlor et al*., 2012]. The magnetic barrier becomes a thicker obstacle in terms of solar wind ion gyroradii, and the solar wind precipitation decreases.

[41] We can compare the results for the precipitation events with the modeling results by *Brecht* [1997] and *Harnett and Winglee* [2006]. They performed simulations with nominal and high values of solar wind density, speed, and IMF strength, and they found that the solar wind precipitation is largest for extreme upstream conditions. These results are consistent with the more frequent observations of solar wind plasma at low altitudes reported during high dynamic pressure conditions [e.g., *Brain et al*., 2005]. However, the models predict that the solar wind precipitation occurs all the time and for any set of upstream conditions. The models and their stationary inputs do not reproduce the intermittent and/or localized solar wind ion precipitation as it is observed [*Diéval et al*., 2012a, 2013; *Stenberg et al*., 2011]. Furthermore, the modelers may simply consider the altitude of the IMB as an indicator of the depth reached by the magnetosheath plasma. In contrast, we made our analysis for intervals of ionosphere without magnetosheath electron spikes, because we want to be sure not to include any low-altitude magnetosheath encounters.

5. Conclusion

[42] We performed a statistical study of precipitating proton and alpha particle events with ~keV energy measured in the Martian dayside ionosphere by Mars Express. We assume that the measured proton and alpha particles come primarily

from the solar wind, although planetary proton precipitation may still be significant according to hybrid models [*Diéval et al*., 2012a, 2012b]. Proton and alpha particle precipitations are found to be intermittent and/or localized, consistent with previous measurements [*Diéval et al*., 2012a, 2012b; *Stenberg et al*., 2011]. We found that the solar wind ion precipitation is less frequent during ICME/CIR encounters: a factor of ~3 for the H^+ precipitation and a factor of ~2 for the He^{2+} precipitation. In addition, the precipitating flux does not increase during pressure pulses.

[43] The total magnetic flux in the magnetic barrier determines the thickness of the magnetic barrier in terms of ion gyroradii and, thus, the effectiveness of the obstacle to the solar wind ion precipitation. We suggest that the total magnetic flux can increase in the magnetic barrier during the impact of a pressure pulse. This is possible since the mass loading of the solar wind by planetary O^+ ions is expected to be stronger during pressure pulses, due to the penetration of the IMF to lower altitudes. The more effective mass loading decelerates the solar wind flow close to Mars. This in turn increases the pileup of the magnetic field on the dayside of Mars, and thus the total magnetic flux increases in the magnetic barrier. The magnetic barrier becomes thicker in terms of solar wind ion gyroradii, which causes the reduction of the H^+ and He^{2+} precipitation during pressure pulses.

[44] **Acknowledgments.** C.D. and G.S. are supported by the Swedish National Graduate School of Space Technology of the Luleå University of Technology. C.D. acknowledges funding from Kungliga Vetenskapsakademien. N.J.T.E. is supported by the Swedish National Space Board. The Swedish contribution to the ASPERA-3 experiment is supported by the Swedish National Space Board.

[45] Philippa Browning thanks the reviewer for assistance in evaluating this paper.

References

Barabash, S., et al. (2006), The Analyzer of Space Plasmas and Energetic Atoms (ASPERA-3) for the Mars Express Mission, *Space Sci. Rev.*, *126*(1-4), 113–164, doi:10.1007/s11214-006-9124-8.

Brain, D. A., et al. (2005), Variability of the altitude of the Martian sheath, *Geophys. Res. Lett.*, *32*, L18203, doi:10.1029/2005GL023126.

Brecht, S. H. (1997), Solar wind proton deposition into the Martian atmosphere, *J. Geophys. Res.*, *102*(A6), 11287–11294, doi:10.1029/97JA00561.

Breus, T. K., et al. (1991), The solar wind interaction with Mars—Consideration of Phobos 2 mission observations of an ion composition boundary on the dayside, *J. Geophys. Res.*, *96*, 11,165–11,174, doi:10.1029/91JA01131.

Chanteur, G. M., et al. (2009), Capture of solar wind alpha particles in the Martian atmosphere, *Geophys. Res. Lett.*, *36*, L23105, doi:10.1029/2009GL040235.

Chaufray, J. Y., et al. (2007), Mars solar wind interaction: Formation of the Martian corona and atmospheric loss to space, *J. Geophys. Res.*, *112*, E09009, doi:10.1029/2007JE002915.

Crider, D. H., et al. (2005), Mars global surveyor observations of the Halloween 2003 solar superstorm's encounter with Mars, *J. Geophys. Res.*, *110*, A09251, doi:10.1029/2004JA010.881.

Diéval, C., et al. (2012a), A case study of proton precipitation at Mars: Mars Express observations and hybrid simulations, *J. Geophys. Res.*, *117*, A06222, doi:10.1029/2012JA017537.

Diéval, C., et al. (2012b), Hybrid simulations of proton precipitation patterns onto the upper atmosphere of Mars, *Earth Planets Space*, *64*, 121–134, doi:10.5047/eps.2011.08.015.

Diéval, C., et al. (2013), A statistical study of proton precipitation onto the Martian upper atmosphere: Mars Express observations, *J. Geophys. Res.*, *118*, doi:10.1002/jgra.50229, in press.

Dubinin, E., et al. (2000), Multi-instrument study of the upstream region near Mars: The Phobos 2 observations, *J. Geophys. Res.*, *105*, 7557–7572, doi:10.1029/1999JA900400.

Dubinin, E., et al. (2006), Plasma morphology at Mars. Aspera-3 observations, *Space Sci. Rev.*, *126*, 209–238, doi:10.1007/s.11214-006-9039-4.

Dubinin, E., et al. (2008), Structure and dynamics of the solar wind/ionosphere interface on Mars: MEX-ASPERA-3 and MEX-MARSIS observations, *Geophys. Res. Lett.*, *35*, L11103, doi:10.1029/2008GL033730.

Dubinin, E., et al. (2009), Ionospheric storms on Mars: Impact of the corotating interaction region, *Geophys. Res. Lett.*, *36*, L01105, doi:10.1029/2008GL036559.

Edberg, N. J. T., et al. (2010), Pumping out the atmosphere of Mars through solar wind pressure pulses, *Geophys. Res. Lett.*, *37*, L03107, doi:10.1029/2009GL041814.

Edberg, N. J. T., et al. (2011), Atmospheric erosion of Venus during stormy space weather, *J. Geophys. Res.*, *116*, A09308, doi:10.1029/2011JA016749.

Fang, X., et al. (2010), Escape probability of Martian atmospheric ions: Controlling effects of the electromagnetic fields, *J. Geophys. Res.*, *115*(A4), A04308, doi:10.1029/2009JA014929.

Frahm, R. A., et al. (2006), Carbon dioxide photoelectron energy peaks at Mars, *Icarus*, *182*(2), 371–382, doi:10.1016/j.icarus.2006.01.014.

Hara, T., et al. (2011), Heavy-ion flux enhancement in the vicinity of the Martian ionosphere during CIR passage: Mars Express ASPERA-3 observations, *J. Geophys. Res.*, *116*, A02309, doi:10.1029/2010JA015778.

Harnett, E. M., and R. M. Winglee (2006), Three dimensional multifluid simulations of ionospheric loss at Mars from nominal solar wind conditions to magnetic cloud events, *J. Geophys. Res.*, *111*, A09213, doi:10.1029/2006JA011724.

Hundhausen, A. J. (1972), *Coronal Expansion and Solar Wind*, Phys. Chem. Space, vol. 5, Springer, New York.

Jian, L., et al. (2006), Properties of coronal mass ejections at one AU during 1995–2004, *Sol. Phys.*, *239*, 393–436, doi:10.1007/s11207-006-0133-2.

Kallio, E., and P. Janhunen (2001), Atmospheric effects of proton precipitation in the Martian atmosphere and its connection to the Mars-solar wind interaction, *J. Geophys. Res.*, *106*, 5617–5634, doi:10.1029/2000JA239.

Kaneda, K., et al. (2009), Solar wind control of the hot oxygen corona around Mars, *J. Geophys. Res.*, *114*, E02007, doi:10.1029/2008JE003234.

Lundin, R., et al. (2004), Solar wind-induced atmospheric erosion at Mars: First results from ASPERA-3 on Mars Express, *Science*, *305*(5692), 1933–1936, doi:10.1126/science.1101860.

McComas, D., et al. (1998), Solar Wind Electron Proton Alpha Particle Monitor (SWEPAM), *Space Sci. Rev.*, *86*(1-4), 563–612, doi:10.1023/A:1005040232597.

McKenna-Lawlor, S., et al. (2012), Magnetic shadowing of high energy ions at Mars and how this effect can be simulated using a hybrid model, *Earth Planets Space*, *64*, 247–256, doi:10.5047/eps.2011.06.039.

Mitchell, D. L., et al. (2001), Probing Mars' crustal magnetic field and ionosphere with the MGS electron reflectometer, *J. Geophys. Res.*, *106*, 23,419–23,427, doi:10.1029/2000JE001435.

Nilsson, H. et al. (2011), Heavy ion escape from Mars, influence from solar wind conditions and crustal magnetic fields, *Icarus*, *215*, 475–484, doi:10.1016/j.icarus.2011.08.003.

Shematovich, V. I., et al. (2011), Protons and hydrogen atoms transport in the Martian upper atmosphere with an induced magnetic field, *J. Geophys. Res.*, *116*, A11320, doi:10.1029/2011JA017007.

Shematovich, V. I., et al. (2013), He^{2+} transport in the Martian upper atmosphere with an induced magnetic field, *J. Geophys. Res. Space Physics*, *118*(3), 1231–1242, doi:10.1002/jgra.50184.

Smith, C. W., et al. (1998), The ACE magnetic fields experiment, *Space Sci. Rev.*, *86*(1-4), 613–632, doi:10.1023/A:1005092216668.

Stenberg, G., et al. (2011), Observational evidence of alpha particle capture at Mars, *Geophys. Res. Lett.*, *38*, L09101, doi:10.1029/2011GL047155.

Vennerstrom, S., et al. (2003), The magnetic field in the pile-up region of Mars, and its variation with the solar wind, *Geophys. Res. Lett.*, *30*(7), 1369, doi:10.1029/2003GL016883.

Vignes, D., et al. (2000), The solar wind interaction with Mars: Locations and shapes of the Bow Shock and the magnetic pileup boundary from the observations of the MAG/ER experiment onboard Mars Global Surveyor, *Geophys. Res. Lett.*, *27*, 49–52, doi:10.1029/1999GL010703.